Journal of Marine Science and Technology

Volume 20 | Issue 6 Article 4

A GEOMORPHOLOGICAL MODEL FOR LANDSLIDE DETECTION USING AIRBORNE LIDAR DATA

Jin-King Liu
Department of Civil Engineering, National Chiao Tung University, Hsinchu City, Taiwan, R.O.C., jkliu@lidar.com.tw

Kuo-Hsin Hsiao
Green Energy and Environment Laboratories, Industrial Technology Research Institute, Hsinchu County, Taiwan, R.O.C.

Peter Tian-Yuan Shih
Department of Civil Engineering, National Chiao Tung University, Hsinchu City, Taiwan, R.O.C.

A GEOMORPHOLOGICAL MODEL FOR LANDSLIDE DETECTION USING AIRBORNE LIDAR DATA

Acknowledgements

This study was supported by the Soil and Water Conservation Bureau, Taiwan in 2010. The authors are also deeply grateful to the Ministry of the Interior for providing LiDAR data acquired in 2005.

Journal of Marine Science and Technology, Vol. 20, No. 6, pp. 629-638 (2012)
DOI: 10.6119/JMST-012-0412-1

A GEOMORPHOLOGICAL MODEL FOR LANDSLIDE DETECTION USING AIRBORNE LIDAR DATA

Jin-King Liu[1], Kuo-Hsin Hsiao[2], and Peter Tian-Yuan Shih[1]

Key words: digital elevation models, geohazards, landscape change, topographic signature.

ABSTRACT

This study analyzes multi-temporal LiDAR data of high accuracy and high resolution by installing a geomorphometric model for extracting landslides. First, two sets of LiDAR data were acquired for before and after a heavy rainfall event. The landslides which took place from 2005 to 2009 were classified automatically by satellite images, and subsequently the landslides were interpreted and edited manually. Geomorphometric parameters including slope, curvature, OHM, OHM roughness, and topographic wetness index were then extracted using stencils of landslide polygons overlaid on respective thematic maps derived from LiDAR, DEM and DSM. The ranges of every parameter were derived from the statistics of the landslide area. Some selected non-morphometric parameters were also included in a later stage to account for all possible features of landslides, such as vegetation index and geological strength. The ranges of the parameters of landslides were optimized for the model by the statistics of the landslide area. The overall accuracy predicted by the model was 64.9%. When the buffer zones of old landslides and riverside areas were included, the overall accuracy was 64.4%, showing no improvement. When landslides smaller than 50 m^2 were filtered, the overall accuracy reached 76.6% and 72.5% for 2005 and 2009, respectively. The results show that the geomorphological model proposed in this research is effective for landslide extraction.

I. INTRODUCTION

Nearly three-quarters of the territory of Taiwan, and 95% of its population, are exposed to frequent natural hazards [7]. In the aftermath of Typhoon Morakot, which dramatically affected southern Taiwan on August 8, 2009, and August 9, 2009, and caused the worst flooding in a century, authorities realized that the country is lacking detailed, accurate, and current elevation data and aerial imagery covering the entire territory of 36000 km^2. To address this problem, a national mapping program, spanning 2010 to 2015, was launched to capture an entire territory of the country with airborne LiDAR (Light Detecting And Ranging) and digital imagery [20]. A LiDAR DEM (Digital Elevation Model) and DSM (Digital Surface Model) and color orthophotos represent a core part of this national spatial data infrastructure.

Taiwan is located on the active collision zone between the Eurasian plate and the Philippine Sea plate. Mountains have a high slope and high relief, and rock formations are highly fractured and fragile. These physiographic settings are unfavorable to slope stabilities. Taiwan is also located on the path of typhoons in northwest Pacific area. Torrential rainfall during the typhoon season often triggers geological hazards. Typhoon Morakot unleashed record rains of 2110 mm in 24 hours with highest record of accumulated rainfalls of more than 3000 mm in southern Taiwan. This caused the worst flooding in a century. The area affected by the typhoon was approximately 10,000 square kilometers. Landslides are one of the most important primary disasters. A national geohazard mapping program employing integrated airborne LiDAR and digital photography was therefore initiated by the Central Geological Survey, Taiwan. This national LiDAR mapping project is dedicated to national geohazard mapping.

In Taiwan, a typhoon can trigger hundreds, even thousands, of shallow landslides in mountainous areas [3, 16, 17]. These landslides can deliver large amounts of sediment into local reservoirs, reducing their water storage capacity [4, 22]. In addition, the turbidity of the water in the reservoirs has a negative effect on the sustainable operation of water supply reservoirs. The assessment and inventory of landslides is essential for effective watershed management and sustainable development. However, because of the steep terrain in Taiwan's mountainous watersheds, most landslides are unreachable. The detailed topographic mapping required for

Paper submitted 12/14/11; revised 03/13/12; accepted 04/12/12. Author for correspondence: Jin-King Liu (e-mail: jkliu@lidar.com.tw).
[1] *Department of Civil Engineering, National Chiao Tung University, Hsinchu City, Taiwan, R.O.C.*
[2] *Green Energy and Environment Laboratories, Industrial Technology Research Institute, Hsinchu County, Taiwan, R.O.C.*

Table 1. The criteria for manual recognition of rainfall-induced landslides.

Photographic Feature	Description	Discrimination rule
Tone	Light, grey light brightness	BV (brightness value) > Threshold
Location	Near ridges, cut-off slopes, road-sides	Trigger events and buffer zone of the feature
Shape	Spoon-shaped, elongated-oval, dendritic, rectangular, triangular	Location-specific and topography-specific
Movement Direction	The drop direction of the landslide is the gravitational vector on the ground surface.	Roughly perpendicular to the streams and topography-specific
Slope	Depend on types of landslides: e.g. (1) Shallow-seated landslides > 45%; (2) Deep-seated landslides ~40%; (3) Debris flows ~10-20%.	Slope > Threshold
Shadow	Depend on whether the landslides are in shadow-side or sunny-side	Solar azimuth in related to slope aspect

emergency mitigation measures cannot be completed within a short period using conventional on-site surveying. Therefore, improving the efficiency and accuracy of landslide monitoring and mapping using remote sensing techniques has become an important research issue [1, 12, 27, 28, 34].

In planning optimal measures of disaster mitigation, researchers often use remote sensing images and digital elevation models to map disaster features and to predict disaster susceptibility. During or immediately after a disaster event, ground survey or photogrammetry, in addition to remote sensing images, can be used to obtain detailed topography data of the subjected area. Because of its ability to obtain high-density point clouds and direct geo-referencing, LiDAR can be used to obtain a more accurate and detailed topographic survey. LiDAR generates accurate 3D coordinates of discrete measurements. Subsequently, DEM and DSM can be produced with high efficiency [23]. In tropical and sub-tropical zones of Taiwan, most of the terrains are covered by dense forestry. Ground surface would be normally predicted by the surface of canopy in photogrammetry if the ground points cannot be seen from two different perspectives of a stereopair. One of the most important advantages of airborne LiDAR compared with conventional photogrammetry is that photogrammetry requires two different lines of sight to both see the same points on the ground from two different perspectives, but LiDAR only needs a single laser pulse to penetrate through the trees to measure the ground beneath. This means that LiDAR will have far fewer areas where the terrain is obscured by trees that block the lines of sight. The images of bare ground before and after the event are thus derived from LiDAR surveys to understand changes in the landscape and their possible consequences. The geomorphometric features become good tools for landslide detection, and are adopted in this study.

The general feature of a rainfall-induced landslide on aerial photograph is a fresh landslide scar with an elongated shape located on a relatively steep slope. Landslides can occur in any kind of geology, as there are some weathered overburdens on steep slopes. In aerial photographs, landslide features include a bright tone, bare surface, and the other features shown in Table 1. Manual interpretation uses both 2D and 3D features of the landslides for recognition: 2D features include tone, location, and shape, and 3D features include location, direction, slope, and shadow effects. A sound consideration of the automation of landslide recognition should consider all these aspects.

Geomorphometry is a major concern in manual interpretation. Geomorphometry, also known as geomorphological analysis, terrain morphometry, terrain analysis, and land surface analysis [11], is the science of quantitative land surface analysis. The purpose of geomorphometry is to extract surface parameters and objects using input from digital terrain models. Pike [25] used a dozen groups of parameters as terrain descriptors by manually digitized digital terrain models. Pike used the resulting "geometric signature or topographic signature" to categorize terrain characteristics, and suggested the degree of landslide danger. Topographic signature of life and their processes are deemed to be strongly influenced by biota [6]. Guth [9, 10] used terrain fabric as measures of a point property of the digital terrain models and the underlying topographic surface. This technique is also called topographic fingerprinting [5], and determines the location of a landslide on the slope. State-of-the-art technology such as high resolution satellite images, digital aerial photography, and airborne LiDAR has opened a new era in the automation of landslide recognition, especially the possibility of applying geomorphometrics. The extraction of land surface parameters is becoming increasingly attractive for both stochastic and process-based modeling, as it makes use of all the levels of detailed digital terrain models. Topographic-based analyses can be used to objectively delineate landslide features, generate mechanical inferences about landslide behavior, and evaluate recent landslide activity [8, 21]. Surface roughness derived from LiDAR DTM allows the objective measurement of landslide topography. Eigenvalues of surface normals are an effective parameter for differentiating shallow landslides and debris flows [38]. Expert knowledge of the geomorphometric properties of landslides may be required to establish an automatic interpretation method. High resolution and high accuracy LiDAR DEM and DSM and orthophotos are now basic constituents of NSDI in Taiwan [20]. Therefore, it is high time to further apply

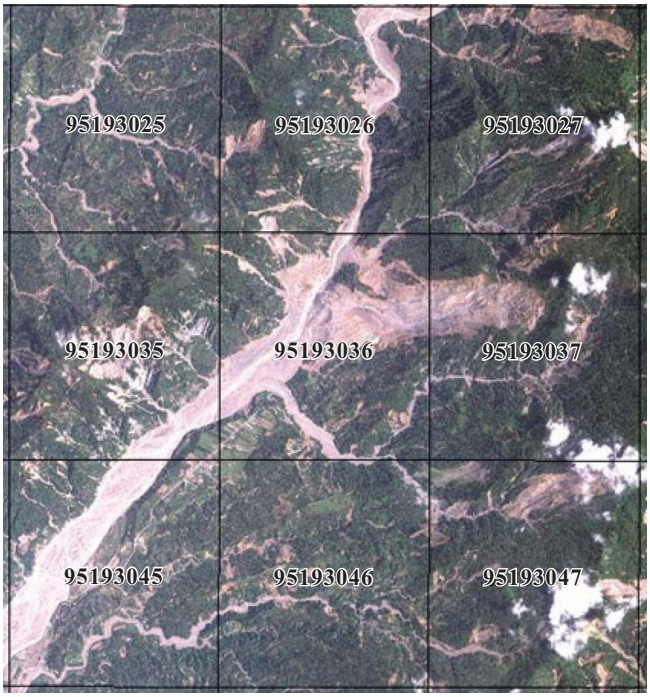

Fig. 1. SPOT image taken on 2009/08/24 after Typhoon Morakot. The 8-digit numbers are the map numbers of national 1/5000 map series.

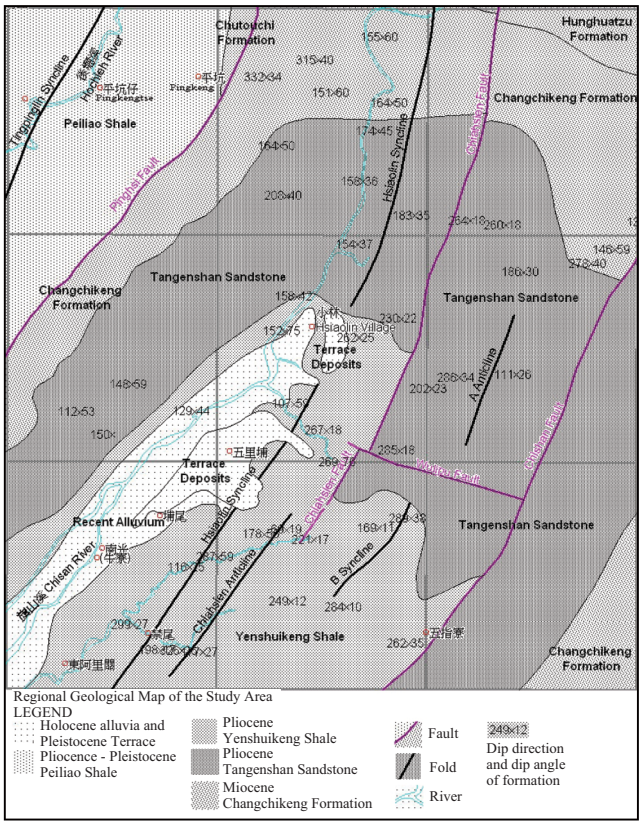

Fig. 2. A regional geological map near the Hsiaolin village [31].

geomorphometry in active landslide study [19].

A geomorphometric model is urgently needed for disaster management. Therefore, the purpose of this study is to develop a geomorphometric model based on highly accurate and high resolution LiDAR topographic data with parameters calibrated by optimized thresholds [33]. The demonstration case in this study was located in southern Taiwan near Hsiaolin village, the village destroyed by Typhoon Morakot. The landslide type which can be detected by this model is a shallow landslide [19].

II. THE STUDY AREA AND DATA COLLECTION

1. Physiographic Settings of the Study Area

Hsiaolin village is located in Chiahsien Township, Kaohsiung City (Fig. 1). The study area is covered by 9 mapsheets of 1/5000 national photomaps: 95193025~95193027; 95193035~95193037, and 95193045~95193047. The village is located on a river terrace of Chisan River. The geological map in Fig. 2 [31] shows that the area is situated in the Western Foothill Zone of Miocene sedimentary formations including Changchikeng Formation, Tangenshan Sandstone, Yenshuikeng Shale, and Peliao Shale. The area is primarily covered by Tangenshan Sandstone and Yenshuikeng Shale. Tangenshan Sandstone consists of alternate layers of sandstone and shale, whereas Yenshuikeng Shale consists of alternations of siltstone and shale with occasional lens-type conglomerates. The river terrace materials include recent fluvial and colluvial deposits of sand and gravel.

2. Satellite Images

This study uses SPOT images taken at approximately the same season as the first LiDAR survey in 2005 used for comparison. The Formosat-2 image taken after Typhoon Morakot was collected and compared with the second LiDAR survey in 2010. In addition, there are several typhoon events from 2007 to 2009. Therefore, this study also uses SPOT images acquired from 2005 to 2009 (Fig. 3) to analyze landslide recurrence rate. The resolution of enhanced-mode SPOT images is 2.5 m, pan-sharpened Formosat-2 image have a resolution of 2.0 m.

3. Airborne LiDAR Data

LiDAR data before and after Typhoon Morakot were collected for this study. The LiDAR feature of multiple returns provides a good means for editing the point clouds and produce DSM, DEM, and CHM (Canopy Height Model) or DBM (Digital Building Model). This in turn enables the analysis of multi-temporal datasets. As Fig. 4 shows, the DEM and DSM in this study are based on 2005 LiDAR survey. The landscape suffered from dramatic changes after Typhoon Morakot (Fig. 5). The large landslide near Hsiaolin Village is the most conspicuous example. Fig. 6 shows the DEM and

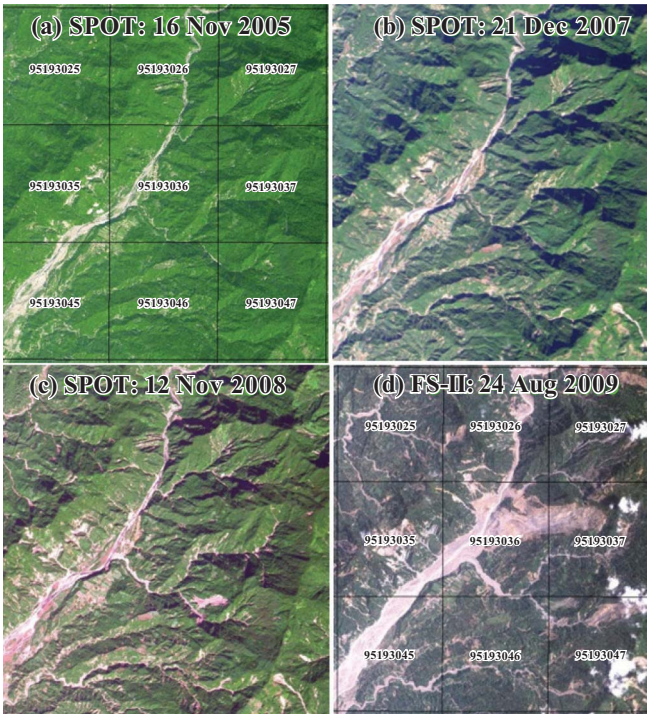

Fig. 3. Satellite images of the study area from 2005 to 2009. Bright grey features on the images are mostly landslide scars. Landslide occurrence increasingly increases in this period of time, as shown in Fig. 8.

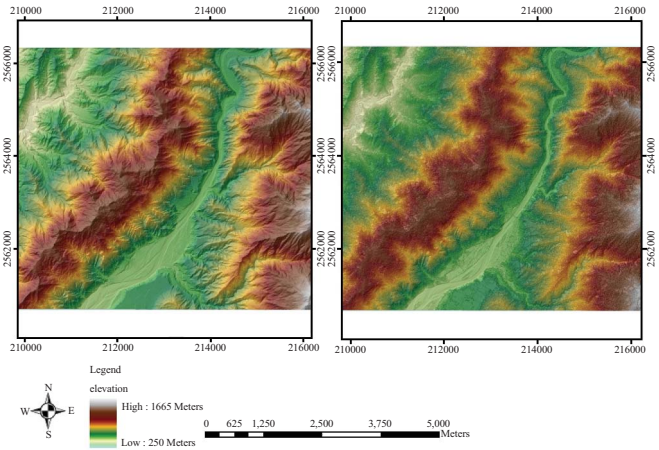

Fig. 4. DEM and DSM images before Typhoon Morakot.

DSM of the study area acquired in 2009 after Typhoon Morakot. Both of the LiDAR datasets in this study were surveyed using a common guideline [23] and a common datum—TWD97 for geodetic coordinates and TWV2010 for vertical system—to maintain the same level of accuracy. The RMSE (Root mean square error) was 16.7 cm with a standard deviation of 16.3 cm for 2005 LiDAR data. The RMSE was 20.2 cm with a standard deviation of 18.3 cm for 2009 LiDAR data. RMSE is a measure of the dispersion between the coordinates obtained by Airborne LiDAR and

Fig. 5. 3D perspective views of Hsiaolin Village before and after Typhoon Morakot. Hsiaolin Landslide has a volume of ~25 million cubic meters with a maximum depth of 85 m on top area and a maximum length of 3,396 m from top to the other side of Chisan River. The landslide completely destroyed the village.

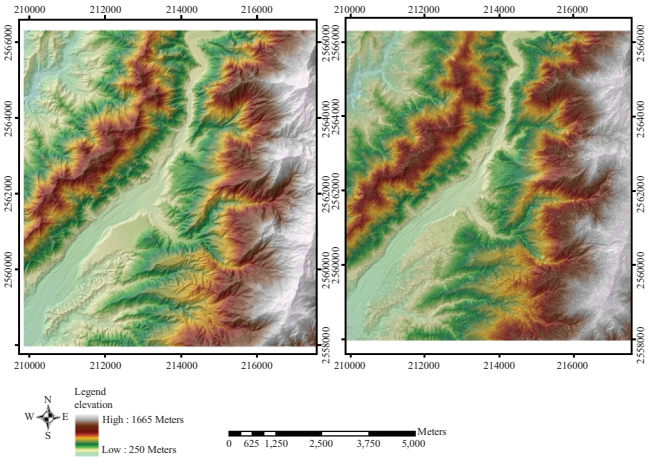

Fig. 6. DEM and DSM obtained after Typhoon Morakot. As compared to those of Fig. 4, dramatic landform change can be found in river valley as well as mountain slopes, especially the example of Hsiaolin Landslide.

those surveyed in the field. Whereas, standard deviation is a measure for the concentration of the differences between these two datasets. The accuracy of these two datasets meets the requirement set in the MOI guideline [23].

III. GEOMORPHOMETRIC MODEL

1. The Geomorphometric Model of Landslides

The proposed model includes both global and local detection procedures, and uses a supervised classification method for global landslide detection. Because of the diversity of the geologic and topographic environments in which landslides occur, omission and commission errors are unavoidable when using the global approach. Thus, local landslide detection is required to increase the accuracy of the resulting landslide map. The local approach employs several interactive manual editing tools to compile landslide information and minimize commission and omission errors. For error analysis, the user accuracy, producer accuracy, average accuracy, and overall accuracy were calculated from a confusion matrix [15].

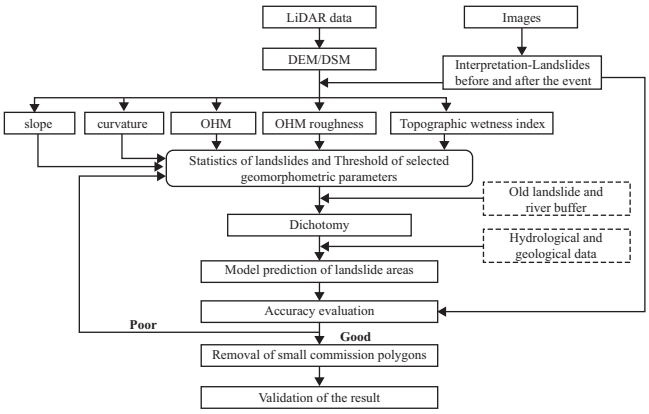

Fig. 7. Flowchart of the geomorphometric model.

Landslide areas possess geomorphometric characteristics that can be used to establish a geomorphometric model to describe the topographic feature of landslides. As the first step, global parameters based on landslides extracted from satellite images by classifying bare land and then filtering out commission errors produced by bare agriculture lands and debris flows were obtained. Landslide polygons were then overlaid on parametric maps derived from 2005 LiDAR data. The parametric parameters of the extracted samples were then used as training sample globally. Thresholds of various parameters were derived based on statistics of the training samples of landslides. Threshold values of the six geomorphometric parameters (T1~T6) were defined a priori based on some user-defined training areas, that is, the landslide polygons. The mean and standard deviation values of each index were calculated and the threshold values were set to be the mean ± 3 standard deviations. The proposed method classifies a pixel as a landslide pixel if the following expression is true: (Slope > T1) ⋂ (Roughness < T2) ⋂ (Curvature > T3) ⋂ (OHM < T4) ⋂ (Greenness < T5) ⋂ (Wetness > T6). Otherwise, it is classified as a non-landslide pixel. Because the global landslide detection algorithm is pixel based, isolated landslide pixels were removed by morphological filtering (e.g., opening and closing). Small landslides were eliminated by setting a minimum mapping unit. Finally, the detected landslide pixels were converted into vector-based polygons. In other words, the pixel conforms to the threshold criterion is designated as 1, otherwise it is designated as 0. The area of the intersecting set of all the parameters was categorized as landslide area. Fig. 7 shows the flowchart of the geomorphometric model established in this study.

2. Geomorphometric Parameters of Landslides

For extracting landslides from high accuracy and high resolution LiDAR data, parameters for establishing the model were selected based on the criteria usually used in manual interpretation of landslides, including the 2D and 3D landslide features detailed previously in Table 1. The parameters of the geomorphometric model in this study were derived from LiDAR DEM and DSM. The major parameters in this model include slope, surface curvature, OHM (object height model), OHM roughness, and topographic wetness index. In addition, NDVI (Normalized Difference Vegetation Index) or greenness is one of the most important indexes for landslide recognition due to that fresh shallow-seated landslides are characterized by bare land without or with little vegetation cover. Therefore, it is also included in the model. A number of vegetation indices, such as the NDVI [13], EVI (Enhanced Vegetation Index) [18], and LAI (Leaf Area Index) [2] have been used in remote sensing for analyzing vegetation cover. Of these indices, NDVI is the standard method for compareing relative biomass and vegetation greenness in remotely sensed images. A higher NDVI indicates a higher level of healthy vegetation cover. The greenness index is similar to the NDVI, except that it substitutes a green band for the near-infrared band.

These parameters are also closely related to the factors for landslide susceptibility [35]. The control factors of slope stability usually include slope angle, strength of materials, and pore water pressure [36]. If the slope gradient is high, the slope can be unstable. Slope angle was thus selected as the first parameter because of its importance, and can be easily derived from DEM. Because DEM represents the bare ground surface and DSM represents the upper envelope of all the objects above the bare ground surface, the difference between these two well-defined surfaces is minimal in the area of rainfall-induced landslide. In this case, the OHM, defined as the difference between these two surfaces, can be a good parameter for automatic landslide recognition. After wash out or sliding, the surface of landslides in nature should be smoother than the surroundings. Surface roughness is an objective and useful measurement of landslide topography [8, 21, 38]. Landform curvature is another critical factor controlling the susceptibility of landslide occurrence [26].

The definition of the parameters is as follows [37, 39]:

(1) Slope. The slope angle of a landslide is the angle between the horizontal surface and the ground surface of the longitudinal axis of the landslide. The slope angle for each landslide can be derived from LiDAR DEM data. A variety of methods are available for terrain slope gradient estimation. However, the details of a high-resolution terrain model may introduce high variations in changes of local slope gradients [30]. This study adopts the method proposed by Parker [24] to overcome this problem, that is the derivatives of the Gaussian function are convoluted with the DEM in the x and y directions, respectively, and then combined to estimate the slope.

(2) OHM. Object height models (i.e., OHMs) are obtained by subtracting DSM from DEM to describe the height of objects above bare ground. The OHM describes the heights of above-ground objects in raster format. Objects close to zero in height may represent the bare soil that characterizes landslides.

(3) OHM Roughness. Roughness is a derivative of OHM, defined as one standard deviation in a 5 × 5 moving window. This measure, which is a function of geological structure and lithology, describes the relief variation in the local area. Because most landslides occur in bare soil areas, the surface is smoother than that of forested areas. Thus, a surface roughness index can be used to detect landslide areas. To account for the high terrain variation in mountainous areas, this study uses object heights rather than surface heights. For simplicity, the standard deviation of object heights within a local window serves as the surface roughness index.

(4) Curvature. Curvature is the second derivative of the surface [29]. Two optional output curvature types are possible: the profile curvature is in the direction of the maximum slope, and the plan curvature is perpendicular to the direction of the maximum slope. The curvature is the slope form and has a significant effect on surface runoff, soil erosion, and deposition processes [32]. This study applies a 15 × 15 medium filter to the DEM to suppress any accidental height changes in the high resolution elevation model. The curvature along the slope direction was then calculated with a 5 × 5 mask.

(5) Topographic wetness index (TWI). Wetness is derived from the concentration of a small watershed [14, 37]. Topography is often one of the major controls of the spatial pattern in saturated areas, which in turn is a key to understanding the variability of hydrological processes. The topographic wetness index has become a widely-used tool to describe wetness conditions. The formula is as follows:

$$\omega = \ln\left(\frac{A}{\tan\theta}\right) \quad (1)$$

where A is the local upslope contributing area and θ is local slope.

(6) NDVI or greenness. This parameter is derived from satellite images or orthophotos acquired at a compatible time as the LiDAR survey. In other words, there are no rainfall events between the time that both the LiDAR data and the images or orthophotos are acquired. Because rainfall-induced landslides of natural slopes are mostly covered by densely-vegetated surroundings, the vegetation index is critical for indicating the areas of bareness. The most popular index is the NDVI:

$$\text{NDVI} = (\text{NIR}-\text{R})/(\text{NIR}+\text{R}) \quad (2)$$

where R stands for the grey value of the red band and NIR stands for grey value of the near infrared band. Theoretically, if the image digital values are calibrated to stand for the reflectance of the target, the NDVI can be widely applicable. However, the digital numbers of the red band and NIR band of digital aerial cameras are not calibrated for this purpose. Therefore, the NDVI value is a relative indicator of vegetation cover. NDVI can be applied to modern digital aerial cameras, which usually include an NIR band. If color aerial photographs include only RGB bands, an alternative greenness parameter can be used. Greenness is also a relative indicator with radiometric values that are not normalized:

$$\text{Greenness} = (\text{G}-\text{R})/(\text{G}+\text{R}) \quad (3)$$

where G is the grey value of the green band, and R is the grey value of the red band. The values of NDVI and Greenness range from -1 to 1. Nevertheless, the range for these values in landslides may change depending on natural weather, terrain conditions and type, and camera sensor settings. A relatively low value implies that the area of the pixel is low vegetated or bare.

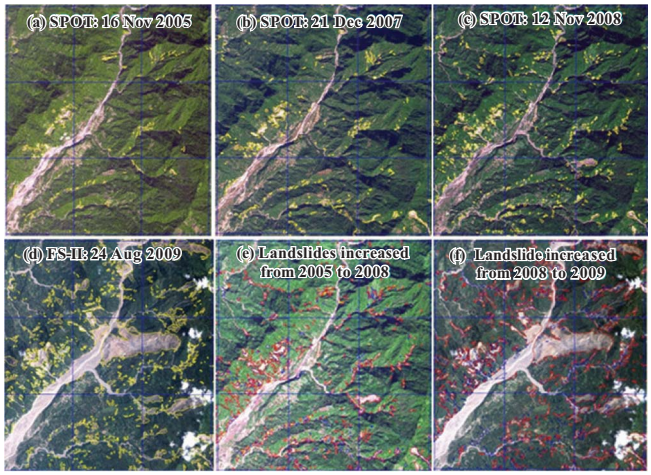

Fig. 8. Landslide distribution between 2005 and 2009. Landslides on images are high-lighted with yellow polylines. New landslides are in red polylines when comparing images taken in 2005 and 2008 (E) and those in 2008 and 2009, respectively.

IV. RESULTS AND DISCUSSION

1. The Geomorphometric Model of Landslides

Bare land has a relatively low reflectance in the infrared region of the electromagnetic spectrum. This feature can be used in unsupervised classification to obtain a preliminary map of landslides. On an interactive screen, manual editing of the results can filter out commission errors such as bare crop fields and debris flows. Fig. 8(a)-8(d) show the distribution of landslides over four different years. Six typhoons affected Taiwan in 2008: Kalmaegi, Fung-wong, Nuri, Sinlaku, Hagupit, and Jangmi. A comparison of the images in 2007 and 2008 reveals more landslides in 2008 (Fig. 8(e)). The number of landslides increased substantially after the torrential rainfall of Typhoon Morakot (Fig. 8(f)).

The recurrence rate of landslides, defined as the repetitive

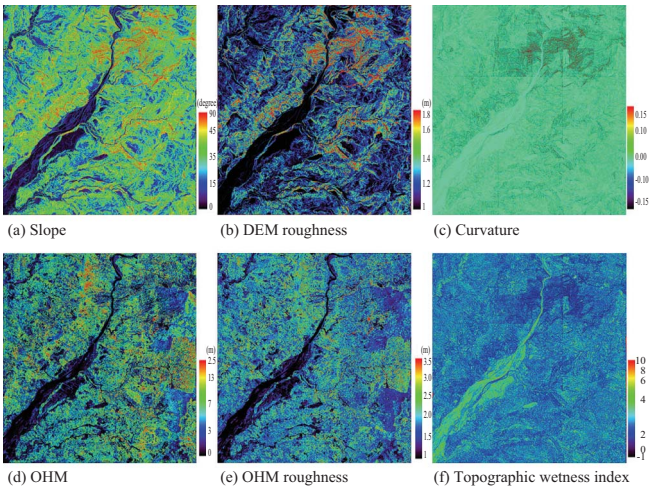

Fig. 9. The distributions of major LiDAR-derived geomorphometric parameters selected for landslide recognition in this study. The coordinates of the maps are (209810, 2566339) and (217609, 2557916) for the lower right and upper left, respectively.

occurrence of landslides between two different times, was 65% between 2007 and 2005. The recurrent rate was even as high as 95.9% between 2009 and 2008. 64.1% of the landslides in 2008 reappeared in 2009 after Typhoon Morakot. The high recurrence rate between succeeding years shows that landslides happen in similar environmental conditions.

To verify the accuracy of the landslides obtained by satellite images, conventional aerial photo-interpretation was conducted. It is shown that the overall accuracy was 92.4% with omission error of 9.2% and commission error of 16.1%.

2. Statistics of Geomorphometric Parameters

Fig. 4 and Fig. 6 are the primary data of DEM and DSM obtained in 2005 and 2009, respectively. For further understanding the features of landforms, geomorphometric parameters have to be extracted from these primary datasets. Fig. 9 shows the distributions of major LiDAR-derived geomorphometric parameters selected for landslide recognition in this study.

Fig. 10 shows the frequency distribution of geomorphometric parameters based on 2005 landslide data. Fig. 11 shows the frequency distribution of these parameters based on 2009 landslide data. The average slope of landslides in 2005 is 31.2 degrees. The surface roughness is generally below 1.5 m, with a cumulative fraction of 90% below 1.5 m (Fig. 10(b)). On basis of the OHM derived from the difference of DSM and DEM, the average OHM is 9.1 m with 20% and 30% of all the landslide pixels having a value below 0.5 m and 3.3 m, respectively. Fig. 10(d) is a frequency distribution of OHM. The major fraction of OHM is distributed between 5 m to 20 m. A cumulative fraction is 37% and 92% for OHM under 5 m and 20 m, respectively. Only 8% of OHM exceeds 20 m, indicating commission errors of trees can be as high as 8%.

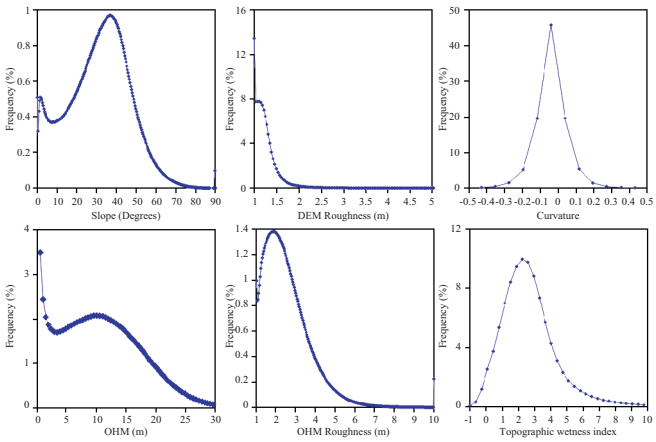

Fig. 10. Frequency distribution of geomorphologic parameters of landslides in 2005.

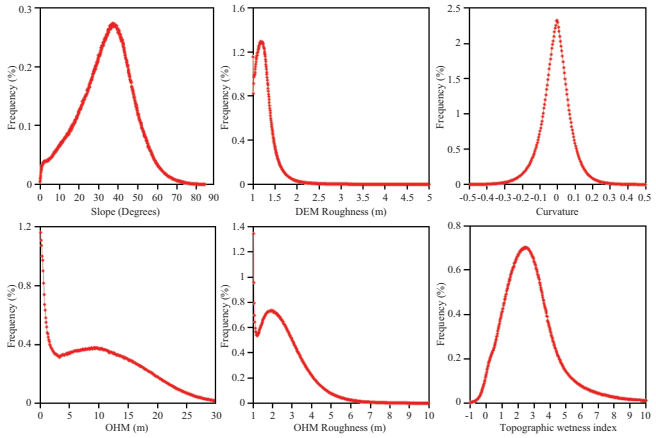

Fig. 11. Frequency distribution of geomorphologic parameters of landslides in 2009.

Fig. 11 shows the frequency distribution of geomorphometric parameters based on 2009 landslide data obtained from images after Typhoon Morakot. In other words, the training samples of the geomorphometric parameters are obtained from the LiDAR data taken in 2009. The average slope of the landslide areas is 33.8 degrees, with a major range in 25~50 degrees. A cumulative fraction is 25% and 90% for slope under 25 and 50 degrees, respectively. The average roughness is 1.2 m, with 90% less than 1.5 m. The average curvature is -0.008, showing that most of the slope forms are more concave than convex. The OHM ranges from 5~20 m with an average of 9.1 m. Similarly, there are 30% of the landslide pixels having an OHM less than 3.3 m. The average roughness of OHM is 2.6 m, with a standard deviation of 1.2 m.

The frequency distributions of various parameters derived by landslides in 2005 and 2009 show no obvious differences. In both cases, the average slopes fall within the range of 30~50 degrees, with a roughness of 1.1~1.7 m, curvature of -0.04~-0.02, OHM under 17 m, and OHM roughness of 1.5~3.5 m.

Table 2. Tries of different combinations of thresholds for model parameters.

tries	slope (degree)	DEM roughness (m)	curvature	OHM (m)	OHM roughness (m)	Wetness	Overall accuracy (%)	Producer accuracy (%)	Omission error (%)	User accuracy (%)	Commission error (%)
1	> 22	< 1.8	> -0.15	< 25	< 4.5	> 0.5	53.59	15.67	84.33	56.45	43.55
2	> 23	< 1.8	> -0.15	< 25	< 4.5	> 0.5	53.81	15.68	84.33	56.1	43.89
3	> 24	< 1.8	> -0.15	< 25	< 4.5	> 0.5	54.22	15.68	84.32	55.46	44.54
4	> 25	< 1.8	> -0.15	< 25	< 4.5	> 0.5	54.72	15.75	84.25	54.93	45.07
5	> 22	< 1.7	> -0.15	< 25	< 4.5	> 0.5	54.95	15.76	84.24	54.58	45.42
6	> 23	< 1.7	> -0.15	< 25	< 4.5	> 0.5	55.35	15.77	84.23	53.94	46.06
7	> 24	< 1.7	> -0.15	< 25	< 4.5	> 0.5	55.91	15.84	84.16	53.31	46.68
8	> 25	< 1.7	> -0.15	< 25	< 4.5	> 0.5	56.14	15.84	84.16	52.97	47.03
9	> 22	< 1.6	> -0.15	< 25	< 4.5	> 0.5	56.55	15.86	84.16	52.32	47.68
10	> 23	< 1.6	> -0.15	< 25	< 4.5	> 0.5	57.16	15.93	84.07	51.61	48.39
11	> 24	< 1.6	> -0.15	< 25	< 4.5	> 0.5	57.09	15.74	84.06	51.26	48.74
12	> 25	< 1.6	> -0.15	< 25	< 4.5	> 0.5	57.8	15.76	84.04	50.62	49.28
13	…	…	…	…	…	…	…	…	…	…	…

When using the landslides in 2008 for training samples, the slope ranges from 25~55 degrees, with an average of 38.2 degrees. As a comparison, the general average slope for 2009 landslides is 33.8 degrees, with an OHM of less than 20 m, roughness less than 1.5 m, and average curvature of -0.018. More concave slope forms were present in 2008 than in 2009. Before the Morakot landslide event, the average OHM was 7.3 m, and the average roughness was 2.4 m with a standard deviation of 1.2 m.

The average slopes of 2008 landslides are higher than those of 2009 landslides. However, the curvature for 2008 is less than that for 2009. There are no obvious differences in OHM and roughness. In 2008, a total of 60% of the landslides have an area of less than 0.5 hectares, whereas the average area of individual landslides in 2009 become larger, with 73% of them possessing an area of less than 1.0 hectare.

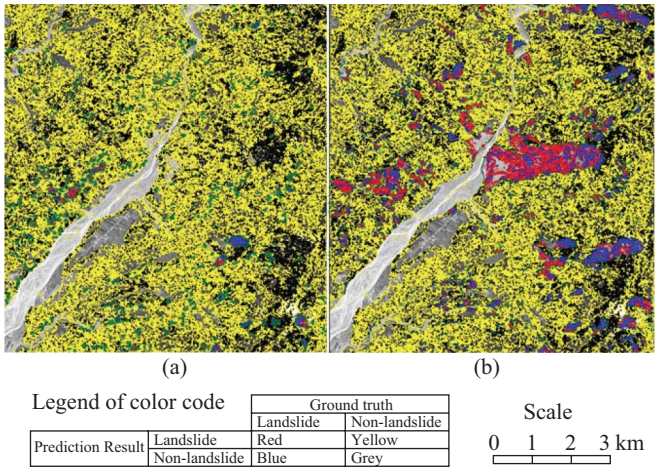

Fig. 12. Landslide prediction with geomorphometric model: (a) Prediction of 2008 landslide susceptibility based on 2005 landslides in vector segments. (b) Prediction of 2009 landslide susceptibility based on 2005 landslides in vector segments.

3. Verification of the Geomorphometric Model

By comparing the spatial distribution of landslides in 2005 and 2009, this study shows that the recurrent rate is as high as 55%. It is therefore reasonable to suppose there is a higher susceptibility in the buffer zone of old landslides. River bank erosion is another important trigger factor for river bank landslides, and upstream erosion has the same effect. Therefore, the proposed model includes buffer zones for river bank and upstream areas. In addition to six geomorphometric parameters, the model includes buffer zones of old landslides and river banks and up-streams.

A sensitivity analysis of the different combinations of thresholds was conducted to find out the optimum combination of thresholds. Tries with major ranges of each parameters have been tested (Table 2). The final optimized results show that the overall accuracy obtained in this study is 68.2%, where the user accuracy is 42.6% and the omission error is 57.4%. Because spatial resolution of DEM and DSM is 1 m, slivers or dispersed isolated small patches of landslides generated when grids are transformed into vectors can be treated as noise. In this study, polygons with an area smaller than 50 square meters are filtered out and manually edited to delete some commission errors, improving the accuracy of the final result. Fig. 12(a) and 12(b) are examples of the modeled results of landslides in 2008 and 2009, respectively. After manual editing, Tables 3 and 4 show that the average accuracies in 2008 and 2009 are 76.6% and 72.5%, respectively. Because landslides only covers small fraction of the study area, the result detected by the model with loose criteria set for the parameter thresholds can be prone to commission errors. This leads to user accuracy as low as 5.0% and 20.2% for 2008 and 2009, respectively. For conservation purposes, commissions cause no big problems, whereas omission errors overlook

Table 3. Model accuracy for 2008 training samples in polygons.

Category	Landslides (hectare)	Non-landslides (hectare)	Producer accuracy (%)	
Landslides	75.54	1,430.51	5.02	Overall accuracy: 76.61%
Non-landslides	105.88	4,957.16	97.91	Average accuracy: 51.47%
User accuracy (%)	41.64	77.61		

Table 4. Model accuracy for 2009 training samples in polygons.

Category	Landslides (hectare)	Non-landslides (hectare)	Producer accuracy (%)	
Landslides	317.18	1,245.36	20.3	Overall accuracy: 72.51%
Non-landslides	560.31	4,446.24	88.7	Average accuracy: 54.19%
User accuracy (%)	36.15	78.12		

hazardous areas. Therefore, this model remains meaningful though further effort is required to filter the commission errors.

V. CONCLUSIONS AND FUTURE RESEARCH

Both of the LiDAR datasets used in this study, including the one obtained from the Ministry of the Interior in 2005 and the one obtained from July 23, 2010, to July 28, 2010, were manually edited for ground points. This editing produced a DEM and DSM grid of 1-m resolution. The parameters of the geomorphometric model were generated using these high resolution data. These parameters include slope, curvature, OHM, OHM roughness, and topographic wetness index. Based on the training samples of landslide polygons in 2009, modeled results give an overall accuracy of 65.8%. Because the recurrent rate from 2005~2009 is more than 55%, the model includes buffer zones of old landslides, river bank, and upstream erosions. To account for sliver noise, polygons smaller than 50 m^2 were filtered out. The accuracies of the model results improved to 76.6% and 72.5% when using training samples of landslide polygons in 2008 and 2009, respectively. These results show that the geomorphological model proposed is effective for landslide extraction.

To improve the model, other physiographical regions should be considered to calibrate the parameters. In addition, more parameters including hydrological conditions and geological environments should be considered to ensure the inclusion of all possible factors of susceptibility. Rainfall is one of the most important factors in hydrological conditions. The critical rainfall and rainfall intensity required to trigger a specific landslide is a challenge for future research. Soil moisture is another important factor in hydrology which might affect landslide occurrence and requires further study. The attitudes of geological formations and the strength of rock bodies are the major factors that should be considered for inclusion in the model.

As the national Taiwanese LiDAR Project progresses, more datasets of multi-temporal and various physiographical settings are becoming available. Future research should investigate the dependence of morphometric parameters on triggering events or geographical locations.

ACKNOWLEDGMENTS

This study was supported by the Soil and Water Conservation Bureau, Taiwan in 2010. The authors are also deeply grateful to the Ministry of the Interior for providing LiDAR data acquired in 2005.

REFERENCES

1. Borghuis, A. M., Chang, K. T., and Lee, H. Y., "Comparison between automated and manual mapping of typhoon-triggered landslides from SPOT-5 imagery," *International Journal of Remote Sensing*, Vol. 28, pp. 1843-1856 (2007).
2. Chen, J. M. and Black, T. A., "Defining leaf area index for non-flat leaves," *Agricultural and Forest Meteorology*, Vol. 57, pp. 1-12 (1992).
3. Cheng, J. D., Huang, Y. C., Wu, H. L., Yeh, J. L., and Chang, C. H., "Hydrometeorological and landuse attributes of debris flows and debris floods during typhoon Toraji, July 29-30, 2001 in central Taiwan," *Journal of Hydrology*, Vol. 306, Nos. 1-4, pp. 161-173 (2005).
4. Dadson, S. J., Hovius, N., Chen, H., Dade, W. B., Lin, J. C., Hsu, M. L., Lin, C. W., Horng, M. J., Chen, T. C., Milliman, J., and Stark, C. P., "Earthquake- triggered increase in sediment delivery from an active mountain belt," *Geology*, Vol. 32, No. 8, pp. 733-736 (2004).
5. Densmore, A. L. and Hovius, N., "Topographic fingerprints of bedrock landslides," *Geology*, Vol. 28, No. 4, pp. 371-374 (2000).
6. Dietrich, W. E. and Perron, J. T., "The search for a topographic signature of life," *Nature*, Vol. 439, pp. 411-418, DOI: 10.1038/nature04452 (2006).
7. Dilley, M., Chen, R. S., Deichmann, U., Lerner-Lam, A. L., and Arnold, M., *Natural Disaster Hotspots: A Global Risk Analysis*, Disaster Risk Management Series No. 5, The World Bank (2005).
8. Glenn, N. F., Streutkera, D. R., Chadwick, D. J., Thackray, G. D., and Dorsch, S. J., "Analysis of LiDAR-derived topographic information for characterizing and differentiating landslide morphology and activity," *Geomorphology*, Vol. 73, pp. 131-148 (2006).
9. Guth, P. L., "Quantifying terrain fabric in digital elevation models," in: Ehlen, J. and Harmon, R. S. (Eds.), *The Environmental Legacy of Military Operations*, Geological Society of America, Reviews in Engineering Geology, Vol. 14, pp. 13-25 (2001).
10. Guth, P. L., "Eigenvector analysis of digital elevation models in a GIS: Geomorphometry and quality control," in: Evans, I. S., Dikau, R., Tokunaga, E., Ohmori, H., and Hirano, M. (Eds.), *Concepts and Modelling in Geomorphology: International Perspectives*, TerraPub, Tokyo, pp. 199-220 (2003).
11. Hengl, T. and Reuter, H. I., *Geomorphometry: Concepts, Software, Applications*, Developments in Soil Science, Vol. 33, Elsevier (2009).
12. Herva, J., Barredo, J. I., Rosin, P. L., Pasuto, A., Mantovani, F., and Silvano, S., "Monitoring landslides from optical remotely sensed imagery: the case history of Tessina landslide, Italy," *Geomorphology*, Vol.

54, Nos. 1-2, pp. 63-75 (2003).
13. Jackson, R. D., Slater, P. N., and Pinter, P. J., "Discrimination of growth and water stress in wheat by various vegetation indices through clear and turbid atmospheres," *Remote Sensing of Environment*, Vol. 15, pp. 187-208 (1983).
14. Kirkby, M. J., "Hydrograph modeling strategies," in: Peel, R., Chisholm, M., and Haggett, P. (Eds.), *Process in Physical and Human Geography*, Heinemann, London, pp. 69-90 (1975).
15. Kohavi, R. and Provost, F., "The case against accuracy estimation for comparing classifiers," *Proceedings of the Fifteenth International Conference on Machine Learning*, Morgan Kaufmann, San Francisco, CA (1998).
16. Lin, C. W., Liu, S. H., Lee, S. Y., and Liu, C. C., "Impacts of the Chi-Chi earthquake on subsequent rainfall-induced landslides in central Taiwan," *Engineering Geology*, Vol. 86, Nos. 2-3, pp. 87-101 (2006).
17. Lin, M. L. and Jeng, F. S., "Characteristics of hazards induced by extremely heavy rainfall in Central Taiwan - Typhoon Herb," *Engineering Geology*, Vol. 58, No. 2, pp. 191-207 (2000).
18. Liu, H. Q. and Huete, A. R., "A feedback based modification of the NDV I to minimize canopy background and atmospheric noise," *IEEE Transactions on Geoscience and Remote Sensing*, Vol. 33, pp. 457-465 (1995).
19. Liu, J. K., Chang, K. T., Rau, J. Y., Hsu, W. C., Liao, Z. Y., Lau, C. C., and Shih, T. Y., "The geomorphometry of rainfall-Induced landslides in Taiwan obtained by airborne LiDAR and digital photography," in: Ho, P. G. P. (Ed.), *Geoscience and Remote Sensing*, InTech, pp. 115-132 (2009).
20. Liu, J. K. and Fei, L. Y., "Taiwanese LiDAR project," *GIM International*, Vol. 25, No. 8, August (2011).
21. Mckean, J. and Roering, J., "Objective landslide detection and surface morphology mapping using high-resolution airborne laser altimetry," *Geomorphology*, Vol. 57, pp. 331-351 (2004).
22. Mikos, M., Fazarinc, R., and Ribicic, M., "Sediment production and delivery from recent large landslides and earthquake-induced rock falls in the Upper Soca River Valley, Slovenia," *Engineering Geology*, Vol. 86, Nos. 2-3, pp. 198-210 (2006).
23. MOI, *Final Report on High Accuracy and High Resolution DEM Mapping and Database Establishment for Selected LiDAR Survey Areas and the Development of Their Applications*, Ministry of the Interior Taiwan, Reported by LiDAR Team of Industrial Technology Research Institute (2006).
24. Parker, J. R., *Algorithms for Image Processing and Computer Vision*, Wiley Computer, New York (1997).
25. Pike, R. J., "The geometric signature: quantifying landslide-terrain types from digital elevation models," *Mathematical Geology*, Vol. 20, No. 5, pp. 491-511, DOI: 10.1007/BF00890333 (1988).
26. Pirotti, F. and Tarolli, P., "Suitability of LiDAR point density and derived landform curvature maps for channel network extraction," *Hydrological Processes*, Vol. 24, pp. 1187-1197, DOI: 10.1002/hyp.7582 (2010).
27. Raju, P. and Saibaba, J., "Landslide hazard zonation mapping using remote sensing and geographic information system techniques - a case study of Pithoragarh area, U. P.," *IEEE 1999 International Geoscience and Remote Sensing Symposium, IGARSS '99 Proceedings*, Vol. pp. 577-579 (1999).
28. Rau, J. Y., Chen, L. C., Liu, J. K., and Wu, T. H., "Dynamics monitoring and disaster assessment for watershed management using time-series satellite images," *IEEE Transactions on Geoscience and Remote Sensing*, Vol. 45, pp. 1641-1649 (2007).
29. Schmidt, J., Evans, I. S., and Brinkmann, J., "Comparison of polynomial models for land surface curvature calculation," *International Journal of Geographical Information Science*, Vol. 17, No. 8, pp. 797-814 (2003).
30. Sharpnack, D. A. and Akin, G., "An algorithm for computing slope and aspect from elevations," *Photogrammetric Engineering*, Vol. 35, No. 3, pp. 247-248 (1969).
31. Song, Q. C., Lin, C. W., Lin, W. X., and Lin, W. Z., *Geological Description of the Geological Map: Chia-Xian in 1/50000 Geological Map Series*, The Central Geological Survey (2000).
32. Stefano, C. D., Ferro, V., Porto, P., and Tusa, G., "Slope curvature influence on soil erosion and deposition processes," *Water Resources Research*, Vol. 36, No. 2, pp. 607-617 (2000).
33. SWCB, *Airborne LiDAR Data for Installing a Landslide Geomorphometric Model - Final Report*, Soil and Water Conservation Bureau, Reported by LiDAR Team of Industrial Technology Research Institute (2010).
34. Tarchi, D., Casagli, N., Fanti, R., Leva, D. D., Luzi, G., Pasuto, A., Pieraccini, M., and Silvano, S., "Landslide monitoring by using ground-based SAR interferometry: an example of application to the Tessina landslide in Italy," *Engineering Geology*, Vol. 68, Nos. 1-2, pp. 15-30 (2003).
35. Tarolli, P., Borga, M., Chang, K. T., and Chiang, S. H., "Modeling shallow landsliding susceptibility by incorporating heavy rainfall statistical properties," *Geomorphology*, Vol. 133, pp. 199-211, DOI: 10.1016/j.geomorph.2011.02.033 (2011).
36. Turner, A. K. and Schuster, R. L., *Landslides: Investigation and Mitigation*, National Research Council, Transportation Research Board Special Report 247, National Academy Press, Washington, D.C. (1996).
37. Wilson, J. P. and Gallant, J. C., *Terrain Analysis*, John Wiley & Sons, Inc. (2000).
38. Woodcock, N. H., "Specification of fabric shapes using an eigenvalue method," *Geological Society of America Bulletin*, Vol. 88, pp. 1231-1236 (1977).
39. Zhou, Q. and Liu, X., *Digital Terrain Analysis*, Science Publisher, Beijing, China (2006).